

# RSC Advances



This is an *Accepted Manuscript*, which has been through the Royal Society of Chemistry peer review process and has been accepted for publication.

*Accepted Manuscripts* are published online shortly after acceptance, before technical editing, formatting and proof reading. Using this free service, authors can make their results available to the community, in citable form, before we publish the edited article. This *Accepted Manuscript* will be replaced by the edited, formatted and paginated article as soon as this is available.

You can find more information about *Accepted Manuscripts* in the [Information for Authors](#).

Please note that technical editing may introduce minor changes to the text and/or graphics, which may alter content. The journal's standard [Terms & Conditions](#) and the [Ethical guidelines](#) still apply. In no event shall the Royal Society of Chemistry be held responsible for any errors or omissions in this *Accepted Manuscript* or any consequences arising from the use of any information it contains.

Cite this: DOI: 10.1039/c0xx00000x

www.rsc.org/xxxxxxx

ARTICLE TYPE

# Hydrogen peroxide treated graphene as an effective nanosheet filler for separation application

Dharupaneedi P. Suhas<sup>a</sup>, Tejraj M. Aminabhavi<sup>b</sup>, Han M. Jeong<sup>c</sup>,  
Anjanapura V. Raghu<sup>d\*</sup>

5

Received (in XXX, XXX) Xth XXXXXXXXXX 20XX, Accepted Xth XXXXXXXXXX 20XX

DOI: 10.1039/b000000x

Graphene has been regarded as an important platform material in developing membranes and has gained a wide range of applications. With the *state-of-the-art* separation technologies, it is highly desirable to develop efficient membranes for organic dehydration that can reduce the recovery costs. In this work, graphene loaded polymer composites of chitosan and poly (vinyl pyrrolidone) for pervaporation (PV) applications because the presence of filler in a polymer matrix would boost membrane performance. Such an enhancement of barrier properties compared to conventional nascent membranes is a result of improved interface compatibility and interaction. In this research, H<sub>2</sub>O<sub>2</sub> treated graphene was used as a nanofiller into chitosan-poly(vinyl pyrrolidone) blend matrix to develop membranes that were tested for PV dehydration of ethanol as a function of filler loading, feed composition and temperature. Physico-chemical interactions between filler nanoparticles and polymer matrix are responsible for improved performance. The prepared membranes have been characterized *via* several analytical techniques. The 2.5 wt.% H<sub>2</sub>O<sub>2</sub> treated graphene loaded composite membrane offered a selectivity of 955, which is almost 40 % higher than those membranes loaded with the same quantity of untreated fillers. Such enhanced membrane performance is attributed to increase in the number of oxygen functionalities on graphene surface after H<sub>2</sub>O<sub>2</sub> treatment, resulting in improved filler interaction at the interface of polymer and graphene in the presence of permeate molecules. Calculations involving Flory-Huggins parameter, diffusion coefficient and Arrhenius activation energy barrier have been performed to explain the PV results in terms of observed increase in membrane performance.

## Introduction

With increasing global demand for renewable fuels and depleting fossil fuel reserves have lead to search for alternate energy sources. Among the vast array of chemicals derived from renewable sources, ethanol is a key platform chemical used in a

*\*Correspondence to: A.V. Raghu (gsraghu2003@yahoo.co.in)*  
wide range of applications. Ethanol obtained from the fermentation of biomass is most often used as a motor fuel or fuel additive to gasoline.<sup>1,2</sup> The production of bio-ethanol essentially involves hydrolysis, fermentation and purification. As per the European Union, fuel grade ethanol should contain at least 98.7 wt.% of ethanol, which makes the purification step crucial.<sup>3</sup>

<sup>a</sup>Materials Science Division, Poornaprajna Institute of Scientific Research, Bengaluru 560110, India. & Department of Chemistry, St. Joseph's College, 36, Langford Road, Bengaluru - 560 027, India

<sup>b</sup>Soniya College of Pharmacy, S.R. Nagar, Dharwad – 580 002, India

<sup>c</sup>Department of Chemistry, University of Ulsan, Ulsan, Republic of Korea-680 749.

<sup>d</sup>Centre for Emerging Technologies, Jain Global Campus, Jain University, Ramanagaram –562 112, India

During purification, 10 wt.% of ethanol (obtained from fermentation) is concentrated up to 99 wt.%, which is fuel grade. However, distillation is good up to 80-85 wt.% of ethanol composition and above which the method becomes prohibitively expensive, especially near azeotropic composition<sup>4,5</sup> and thus a major share of production cost goes to alcohol purification. On

the other hand, membrane-based pervaporation (PV) offers an alternative approach with advantages of low energy consumption, low operating cost and excellent performance in dehydrating ethanol at azeotropic compositions.<sup>6</sup> The method is vital to enhance ethanol composition from 80-85 wt.% up to 99 wt.%, but key to this success relies on developing suitable membranes that can offer simultaneously high flux and selectivity along with a good thermo-mechanical strength.<sup>7,8</sup>

Hydrophilic polymers such as sodium alginate, chitosan (CS), poly(vinyl alcohol), polyacrylonitrile and polyimide have been widely used in the earlier literature.<sup>9</sup> Among these CS, a biopolymer obtained from the crustacean shells and has good film forming ability, moderate mechanical strength as well as excellent affinity towards water, is regarded as one of the indispensable materials for PV dehydration of organics.<sup>10</sup> Poly(vinyl pyrrolidone) (PVP), is another hydrophilic biopolymer having excellent compatibility with CS forming a homogeneous blend matrix.<sup>11</sup> Earlier research reported that blending of PVP with CS can influence the PV performance of membranes.<sup>12,13</sup>

It has been realized that performance of chitosan for extended use can be reduced due to its swelling characteristics. To avoid this issue, various methods such as blending, crosslinking etc., have been attempted. Even compared to such membranes, recent trends of developing nanocomposite membranes prepared by incorporating nanofillers into a polymer matrix seem to offer improved physical, chemical and separation properties. Such nanocomposite membranes combine the flexibility of polymers with the strength and specificity of inorganic fillers.<sup>14</sup> Typical fillers used in developing nanocomposite membranes are usually hydrophilic, porous or intercalated materials, whose presence creates tortuous pathways in a matrix, thus favouring selective permeation of smaller molecules such as water.<sup>15</sup> Some of the widely used fillers in this category are clay,<sup>16,17</sup> heteropolyacids,<sup>18</sup> zeolites,<sup>19</sup> single-walled alumina-silicate nanotubes,<sup>20</sup> zeolitic imidazolate frameworks (ZIFs),<sup>21</sup> titanate nanotubes,<sup>22</sup> carbon nanotubes<sup>23</sup> and graphene.<sup>24</sup>

Graphene is a two dimensional crystalline allotrope of carbon with densely packed carbon atoms arranged in a regular hexagonal  $sp^2$  bonded atomic scale chicken wire pattern. In recent years, graphene has created a greater interest as a versatile

nanosheet material due to its exceptional electron transport capacity, superior mechanical strength and high surface area.<sup>25</sup> These properties have been prompted researchers to develop nanocomposite polymeric membranes containing graphene.<sup>26-32</sup> Earlier, Nair<sup>33</sup> et.al., and Hung<sup>34</sup> et.al., used submicron thick membranes of graphene oxide (GO) for separating various solvents, which showed superior selectivity to water compared to organics. Unfortunately, practical applications of these membranes are limited due to high cost involved in graphene production. An effective approach would therefore be to use graphene as filler in a polymer matrix to develop graphene-loaded nanocomposite membranes. However, uniform dispersion of graphene in to a polymer matrix is somewhat difficult, yet previous efforts have been fruitful.<sup>24,35</sup> Basically, presence of hydroxyl, carboxyl and epoxide groups on graphene surface would achieve electrostatic and H-bonded interactions with polymer matrix. It is thought that if we use oxygen containing functional groups onto graphene surface, it would enhance interfacial interaction between polymer structure and nanosheets of graphene, consequently resulting in enhanced membrane performance.

In efforts to enhance interface interactions between graphene and chitosan polymer, we have treated graphene with hydrogen peroxide, which introduces additional oxygen functionalities onto graphene surface. While using these nanofillers to prepare nanocomposite blend membranes of chitosan/PVP, the presence of PVP is expected to facilitate filler dispersivity. The prepared nanocomposite membranes were tested for PV dehydration of ethanol. The interaction between graphene oxide and polymer matrix was assessed by Fourier transform infrared spectroscopy (FTIR), field emission scanning electron microscopy (FE-SEM), wide angle X-ray scattering (WAXS) and contact angle measurements. Furthermore, membrane performance was evaluated by sorption, diffusion and Arrhenius activation energy parameters.

## Experimental

### Materials and methods

The natural graphite (HC-908) was procured from Hyundai Coma Co. Ltd., Mumbai, India. Chitosan and poly(vinyl pyrrolidone) polymers were purchased from SRL chemicals, Mumbai, India. Glacial acetic acid (100%), concentrated HCl

(35%), nitric acid, potassium chloride and glutaraldehyde were all procured from s. d. fine chemicals, Mumbai, India. Absolute ethanol (EtOH) (99.9%) was obtained from Commercial Alcohols, Brampton, Canada. All other chemicals used in this work were of reagent grade and used without further purification (unless specified). Double-distilled water was used throughout the research.

### Preparation of functionalized graphene sheets

Graphite oxide was prepared by a modified Brondie method as reported by Jeong<sup>36</sup> et.al. In a typical procedure, 10 g of nascent graphite was taken in a 500 mL round bottom flask to which 200 mL of ice cooled fuming nitric acid was added. Subsequently, the reactants were mixed overnight and transferred to a beaker containing 3 L of double distilled water. The product thus obtained was filtered and washed with copious amount of water to neutralize. The graphite oxide has the empirical formula:  $C_{10}O_{3.45}H_{1.58}$  (as per elemental analysis). Dried graphite oxide was introduced into quartz tube maintained under an inert atmosphere. The quartz tube was introduced into a furnace maintained at 1100°C, where layers of graphite oxide disintegrate into individual graphene sheets. Thus prepared graphene has the empirical formula:  $C_{10}O_{0.78}H_{0.38}$  with a surface area of 428 m<sup>2</sup>/g.

### H<sub>2</sub>O<sub>2</sub> treatment on graphene sheets

In order to enhance oxygen functionality, graphene was immersed in an excess amount of H<sub>2</sub>O<sub>2</sub> solution (30 wt.% concentration) and the mixture was sonicated for 1 h followed by stirring for 3 h at 60°C. The products were filtered and washed with excess amount of double distilled water followed by acetone washing and dried at 100°C in a hot air oven for 24 h. Thus obtained graphene showed enhanced oxygen content as per the empirical formula:  $C_{10}O_{0.99}H_{0.73}$  and is designated as graphene oxide (GO)<sup>36</sup>. The enhanced oxygen functionality is expected to increase the compatibility of graphene with chitosan matrix. The morphology of GO was examined by TEM, XRD, FTIR and BET studies.

### Membrane Fabrication

All the blend membranes containing 10 wt.% of PVP in CS and loaded with GO as a nanofiller were prepared by solution casting followed by solvent evaporation. First, chitosan solution

was prepared by mixing chitosan powder with acetic acid and water in the ratio of 3:3:94. Then, PVP solution prepared in water media was added to the above mixture, stirred on a magnetic stirrer and allowed to stand for overnight to get rid of air bubbles. The required quantity of GO (1, 2, 2.5 and 3 wt.%) was agitated and sonicated for 2 h with water before adding into CS-PVP blend solution that was stirred on a magnetic stirrer for 24 h to achieve uniform dispersion. The resulting mixture was poured onto a perfectly aligned clean glass plate kept in a dust free environment and allowed to dry at the ambient temperature.

Dried membranes were immersed in a cross-linking bath for 2 h containing water-acetone mixture in the ratio 3:7 along with 2 mL of glutaraldehyde as a cross-linking agent and 1 mL of HCl as a catalyst. In order to remove the unreacted glutaraldehyde, membranes were alternatively rinsed with water and methanol for about 4-5 times followed by soaking in methanol for 24 h. Using the above procedure 1, 2, 2.5 and 3 wt.% of GO loaded CS-PVP blend nanocomposite membranes were prepared and these were designated as CS-PVP-1, CS-PVP-2, CS-PVP-2.5 and CS-PVP-3, respectively. Nascent CS (crosslinked, but without adding filler) and CS-PVP-2.5 (U) (CS-PVP by adding 2.5 wt.% of untreated graphene) were fabricated as control membranes for comparison purposes.

### Membrane Characterization

The chemical interactions between functional groups of GO and CS-PVP blend matrix was assessed by FTIR. All measurements were done in a transmission mode in the range of 400-4000 cm<sup>-1</sup> using Bruker Alpha-T spectrophotometer. Each sample was scanned for 32 times with a resolution of 4 cm<sup>-1</sup>. Prior to this, the sample pellets were prepared by applying a hydraulic pressure of 400-450 kg cm<sup>-2</sup> on a mixture containing dried KBr and the sample.

Solid state morphology of the membranes was analyzed using the Bruker D-2 phaser X-ray diffractometer. The Cu-K $\alpha$  radiation source was used to generate X-rays of wavelength 1.5406 Å. The powder samples were scanned in the range of 2 $\theta$  of 5°-60° at the scanning rate of 2° min<sup>-1</sup>.

The micro-morphology and thickness of the nanocomposite membranes were assessed by FE-SEM (Field Emission Scanning Electron Microscopy) Zeiss Ultra-55 instrument. In order to

enhance the image quality, membranes were coated with a conductive layer of sputtered gold of 0.5-1  $\mu\text{m}$  thickness.

Thermal stability and degradation patterns of all the membranes were evaluated by thermogravimetry (TQ-500) performed in the temperature range of 40-600°C under slow heating rate of 10°C  $\text{min}^{-1}$  in inert atmosphere by flowing nitrogen gas at a constant rate of 50  $\text{mL}\cdot\text{min}^{-1}$ . For each analysis, approx. 5-8 mg of the sample was taken in aluminium pan and thermal stability was analyzed.

Mettler Toledo (DSC-822) instrument was used to obtain DSC (differential scanning calorimetry) thermograms of the membranes. The aluminum pans were conditioned before start of the experiment. About 10 mg of the sample was sealed in an aluminum pan and measurements were taken from the ambient temperature to 250°C with a ramp rate of 10°C  $\text{min}^{-1}$  by maintaining inert atmosphere through constant supply of nitrogen gas at a flow rate of 50  $\text{mL}\cdot\text{min}^{-1}$ .

The relative surface hydrophilicity of the membranes was measured by a static water Sessile-drop contact angle instrument (Data Physics OCA-20) at 25°C. Membrane samples were vacuum dried prior to contact angle measurements. Membranes were adhered to suitable glass surface, onto which 2  $\mu\text{L}$  of deionized water droplet was placed and its image was photographed at exactly 10 s using a CCD camera. All the reported values are averages of five measurements taken at different places by considering standard deviations of  $\pm 3\%$ .

Equilibrium swelling experiments were performed gravimetrically at 30°C by soaking circularly-cut membrane samples (2.5 cm dia) in 10wt.% of water containing feed mixture. Initial weight of the membrane was noted as  $W_d$ . These membranes were immersed in air tight test bottles containing 30  $\text{cm}^3$  of feed mixtures for 48 h. Then, membranes were removed from the test bottles, wiped-off with soft tissue paper wraps to remove the surface-adhered liquid droplets and swollen weight was noted as  $W_s$ . From these data, % equilibrium swelling was calculated as<sup>37</sup>:

$$\text{Equilibrium Swelling (\%)} = \left( \frac{W_s - W_d}{W_d} \right) \times 100 \quad \text{----- (1)}$$

### Pervaporation Experiments

An indigenously designed stainless steel unit was used to carry out PV experiments<sup>38</sup>. The set-up had two compartments

*viz.*, feed tank and permeate cell. The membrane with an effective area of  $3.84 \times 10^{-3} \text{ m}^2$  was placed tightly between two O-shaped teflon rings, which was further placed onto a porous stainless steel support. The feed tank was double-walled cylindrical shaped stainless steel equipment with a maximum capacity of 500 mL. Through its outer jacket, warm water from a thermostatic bath (Grant UK Model GD-120) was circulated to maintain the desired temperature at the feed tank, which was provided with a stirrer and a thermometer; the feed mixture was maintained at atmospheric pressure (760 mmHg), while permeate was maintained at  $> 5$  mbar pressure with the help of Telstar double stage suction pump. To attain constant flux, membranes were equilibrated with the feed mixture for 2 h prior to starting the experiment. Permeate samples were collected at regular intervals of time using two glass traps immersed in a liquid nitrogen containing Dewar flask.

Samples were collected at intervals of 1 h and its weight was measured on a Sartorius BSA 224 balance, while compositions of feed and permeate samples were measured by refractometer as well as by gas chromatography (GC). Refractive index was measured using Mettler Toledo Refractometer to an accuracy of  $\pm 0.0001$  units and % composition of permeate mixture was estimated with the help of previously established calibration curve of refractive index vs known composition of the mixture at  $30 \pm 0.1^\circ\text{C}$ . To reconfirm permeate compositions, the GC runs were made on a Thermofisher Trace-700 coupled with a Porapak Q column and TCD detector. In this, 1  $\mu\text{L}$  of the sample was injected along with nitrogen carrier gas at a flow rate of 1.5  $\mu\text{L}\cdot\text{min}^{-1}$  at the oven temperature of 150°C. For each sample, three separate readings were taken, but average values of three independent measurements were considered to an accuracy of  $\pm 3\%$  standard error. Membranes were stable for more than 10 h of continuous PV operation.

As recently pointed out<sup>39</sup>, normalizing the flux with respect to driving force would make the comparison of PV data more meaningful. It may significantly decouple the effect of operating conditions on performance evaluation, while at the same time quantify the contribution by the nature of the membrane its separation efficiency. In this work, as noted previously<sup>40,41</sup> the driving force normalized parameters *viz.*, permeability ( $P_i^G$ ) and selectivity ( $\alpha_{ij}$ ) values proposed by Baker and Wijmans<sup>42</sup> are used to treat the PV data as these appear to be more appropriate to

represent PV results in a more meaningful manner. Moreover, such data can be comparable directly with the literature findings. This prompted us to compute permeability ( $P_i^G$ ) using:

$$P_i^G = D_i K_i^G = j_i \left( \frac{l}{p_i^f - p_i^p} \right) \quad \text{----- (2)}$$

where subscript  $i$  represents either ethanol or water,  $K_i^G$  and  $D_i$  are sorption and diffusion coefficients of  $i^{\text{th}}$  component, respectively;  $j_i$  is molar flux of the  $i^{\text{th}}$  component;  $p_i^f$  and  $p_i^p$  are  $i^{\text{th}}$  component vapor pressure of feed and permeate mixtures, respectively;  $l$  is membrane thickness (82  $\mu\text{m}$ ). The permeability values are reported in Barrer (1 Barrer =  $1 \times 10^{-10} \text{ cm}^3 \text{ (STP) cm/cm}^2 \text{ s cmHg}$ ). Using flux ( $J_i$ ) values in  $\text{g/m}^2\text{h}$  obtained from PV experiment, the molar volume ( $v_i$ ) [22.41 (STP)/mol] and molecular weight ( $m_i$ ) of the  $i^{\text{th}}$  component, the molar flux ( $j_i$ ) was calculated as:

$$j_i = \left( \frac{J_i v_i}{m_i} \right) \quad \text{----- (3)}$$

The partial vapor pressure ( $p_i^f$ ) was calculated using van Laar equation:

$$p_i^f = x_i \gamma_i p_i^s \quad \text{----- (4)}$$

Here,  $p_i^s$ ,  $\gamma_i$  and  $x_i$  are saturated vapor pressure, activity coefficient and molar concentration, respectively of the  $i^{\text{th}}$  component. Antoine equation<sup>43</sup> was then used to calculate saturated vapor pressure,  $p_i^s$  as:

$$\log p_i^s = \left( \frac{A - B}{T + C} \right) \quad \text{----- (5)}$$

where  $T$  is temperature in degree Kelvin, while  $A$ ,  $B$  and  $C$  are Antoine constants obtained from literature<sup>44</sup>. The membrane selectivity ( $\alpha_{ij}$ ) was calculated as the ratio of permeabilities of components,  $i$  (water) and  $j$  (EtOH).

$$\alpha_{ij} = \frac{P_i^G}{P_j^G} \quad \text{----- (6)}$$

## Results and Discussion

### Characterization of graphene oxide (GO)

TEM images of GO shown in **Figure 1a and b** reveal dark thin crumpled paper-like surface with many fibrous type of wrinkles and folding, which are characteristics of graphene sheets<sup>45</sup>. In order to examine the % composition of oxygen onto the graphene surface, SEM-EDX analysis was performed as shown in **Figure 1c and d**, wherein green dots on the surface are attributed to the presence of oxygen, revealing highly oxygenated surface. The presence of oxygen containing functional groups is also evident from the examination of FTIR spectrum given in **Figure 1e**, where absorption bands are observed at 3430, 1540 and 1230  $\text{cm}^{-1}$  related to oxygen containing functional groups of GO.

The 2D (0 0 2) sheet like structure of graphene was marked with the appearance of XRD peak at  $2\theta$  of  $26.3^\circ$  (as seen in **Figure 1f**) showing the d-spacing of 0.339 nm. The surface area of graphene as measured by BET isotherm was 428  $\text{m}^2/\text{g}$ , revealing six-layered structure. The elemental analysis confirms that after  $\text{H}_2\text{O}_2$  treatment, oxygen content increased from  $\text{C}_{10}\text{O}_{0.78}\text{H}_{0.38}$  to  $\text{C}_{10}\text{O}_{0.99}\text{H}_{0.73}$ . All these unique observations are the attributes of graphene, which are expected to enhance the overall performance of the nanocomposite membranes in PV dehydration of ethanol.

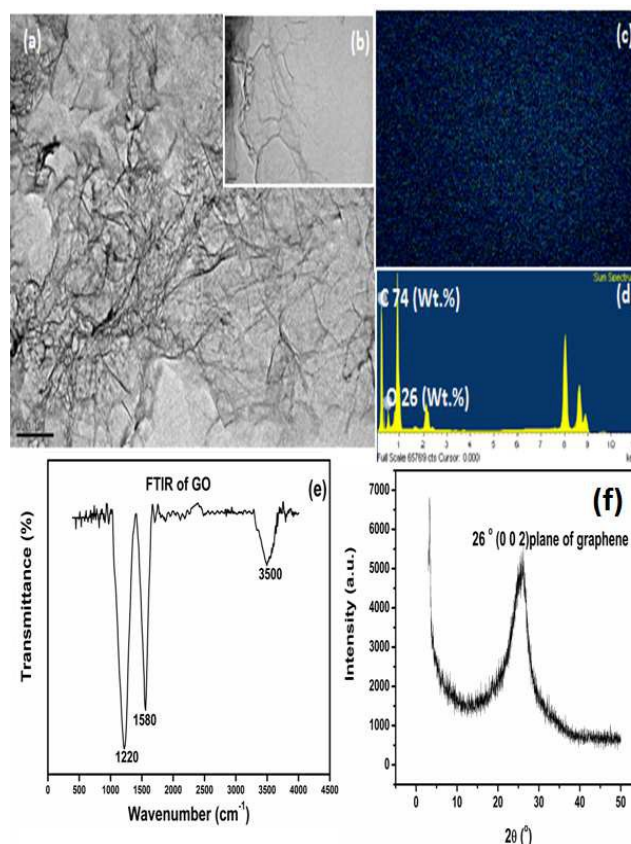


**Fig. 1** (a): TEM image of GO; (b) (in-set) showing image at higher resolution; (c) EDX-image of GO; (d) EDX analysis showing weight % composition of GO; (e) FTIR spectrum of GO; (f) XRD of GO.

## 5 Characterization of Membranes

### Fourier transform infrared spectroscopy (FTIR)

FTIR spectra of nascent CS-PVP and its GO incorporated nanocomposite membranes are presented in **Figure 2**, wherein all the spectra are shifted upwards to avoid overlapping. FTIR spectrum of nascent CS-PVP shows multiple absorption bands in the region 400-4000  $\text{cm}^{-1}$ , which are in accordance with the reported spectra by Magalad<sup>18</sup> et. al. The combined characteristic broad peak of -OH and -NH<sub>2</sub> groups was observed around 3400-3500  $\text{cm}^{-1}$ . Interestingly, these peaks show a red shift with increasing filler loading, signifying effective hydrophilic linkage between the filler particles and the polymer blend matrix.

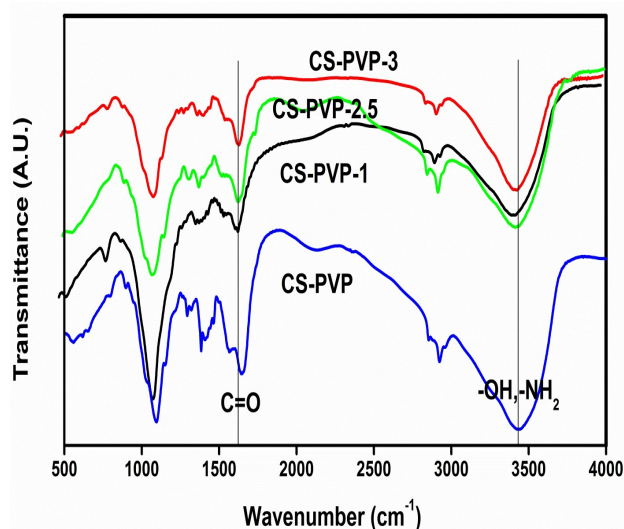


**Fig. 2** FTIR of nascent CS-PVP and its composites with different loading of GO, showing an increase in red-shift with increasing GO loading.

### Wide angle X-ray scattering (WAXS)

**Figure 3** depicts WAXS tracings of nascent CS-PVP and its nanocomposites, showing two characteristic peaks. The first sharp peak observed at  $2\theta$  of 10-12°, and the second weak peak observed at 18-22°, are in agreement with the reported data<sup>13</sup>. With an increase in GO loading, the peak intensity gradually decreased due to molecular level interaction between GO and CS/PVP, leading to disturbance in the ordered arrangement of CS chains, consequently resulting in a decrease of peak intensity. This observation indicates fine molecular level dispersion of GO

nanosheets in the CS/PVP matrix and this might have facilitated the tortuous pathways in the matrix, thereby favouring selective diffusion of water molecules over that of ethanol. This can be further confirmed by the non-appearance of GO peak.

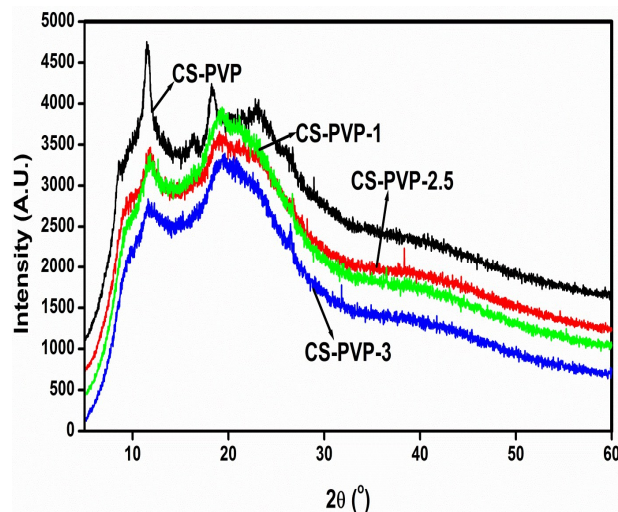


**Fig. 3** XRD of nascent CS-PVP and its composite membranes with different loadings of GO, showing a decrease in peak intensity with increasing GO loading.

### 45 Field Emission Scanning Electron Microscopy (FE-SEM)

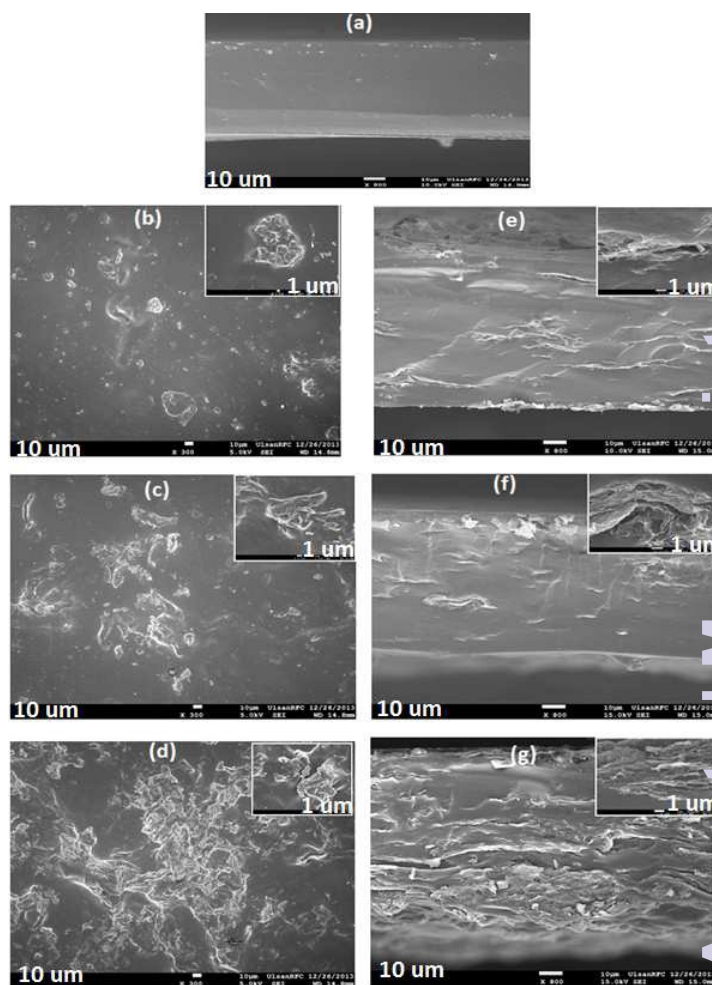
To observe the dispersion of GO nanosheets at higher resolution and to obtain additional information on the interfacial interaction between GO and the polymer matrix, SEM images were taken. The cross-sectional view of nascent CS/PVP blend is as shown in **Figure 4a**, which appears much darker due to non-conductive nature of CS/PVP towards electrons. Obviously, brighter spots observed in GO loaded CS/PVP blend-composite membranes as shown in **Figure 4(b-g)** are attributed to the presence of GO sheets. Both cross-sectional and the top views of nanocomposite membranes were obtained. **Figures 4(e, f, g)** shows cross-sectional SEM of CS-PVP-1, CS-PVP-2.5 and CS-PVP-3, respectively. These images are densely packed with groves due to differential interaction between GO and CS-PVP matrix.

The top surface of all the GO incorporated CS/PVP membranes are shown in **Figures 4(b, c, d)**. These images show rougher surface as against smoother surfaces observed for nascent CS/PVP membrane. Notice that presence of bright spots increases with GO loading. The higher resolution image as shown in insets of **Figures 4(b, c, d)** reveal individual particle dispersion with CS-PVP-1 and CS-PVP-2.5 membranes, but CS-PVP-3 membrane showed micro-agglomeration. These observations

suggest that membranes seem to be reaching an optimum performance limit at around 2.5 wt.% loading, and above this loading limit, particles start agglomerating, thus resulting in reduced performance. Since the GO nanosheets are well dispersed in the membrane blend matrix, and hardly any individual nanosheets could be seen, confirming superior interfacial interaction. The average membrane thickness was estimated to be around 82  $\mu\text{m}$ .

### 10 *Thermogravimetric Analysis (TGA)*

Thermal analysis of all the membranes were performed in the temperature range of 40-600°C in inert nitrogen atmosphere, and the results displayed in **Figure 5a** showed combination of release of moisture followed by breaking of polymer chains. The first major weight loss occurred at 100°C, due to the release of moisture. The second major weight loss of about 30-40 wt.% occurred at 230°C, which can be attributed to polymer chain degradation. Thus by increasing GO loading, thermal stability improved, indicating favourable interface interaction between GO and the polymer blend matrix.



25 **Fig. 4** FE-SEM (top-view) of (b) CS-PVP-1, (c) CS-PVP-2.5, (d) CS-PVP-3; FE-SEM (cross-sectional view) of (a) nascent CS-PVP (e) CS-PVP-1, (f) CS-PVP-2.5 and (g) CS-PVP-3; (in-set) showing SEM images at higher resolution.

### 30 *Differential scanning calorimetry (DSC)*

DSC analyses of all membranes were performed from 40 to 350°C under nitrogen (inert) atmosphere and thermograms are presented in **Figure 5b**. An endothermic curve from 96 to 130°C, whereas exothermic curve in the temperature range of 255 to 275°C are observed. The endothermic curve is mainly due to the release of absorbed water molecules, while exothermic curve is due to polymer chain degradation at higher temperature. With increasing GO loading, both endothermic and exothermic curves shifted to higher temperature, indicating enhanced water holding capacity and thermal stability of the membranes.

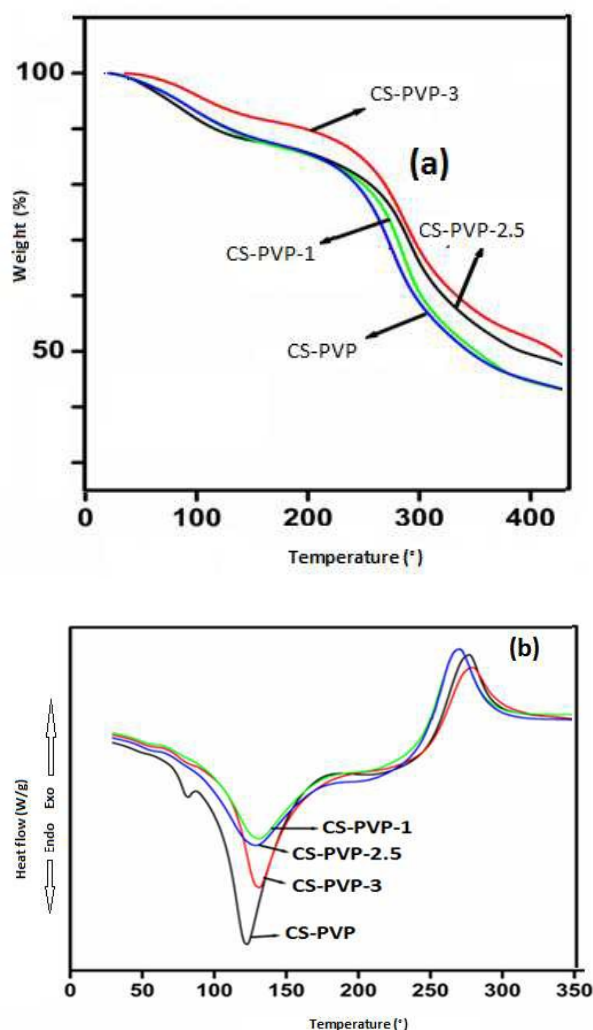


**Fig. 5** Thermal analysis of nascent CS-PVP, CS-PVP-1, CS-PVP-2.5 and CS-PVP-3 using (a) non-oxidative TGA curves and (b) DSC thermograms.

### Contact angle Studies

Water contact angle is typically used for estimating the relative hydrophilicity of membranes. Membranes with smaller values of contact angle are more hydrophilic and *vice-versa*. The effect of GO loading on membrane hydrophilicity is shown in Figure 6, where we find a systematic increase in membrane hydrophilicity with increase in GO loading. This is attributed to enhanced surface hydrophilicity and roughness due to GO loading, into the polymer matrix.

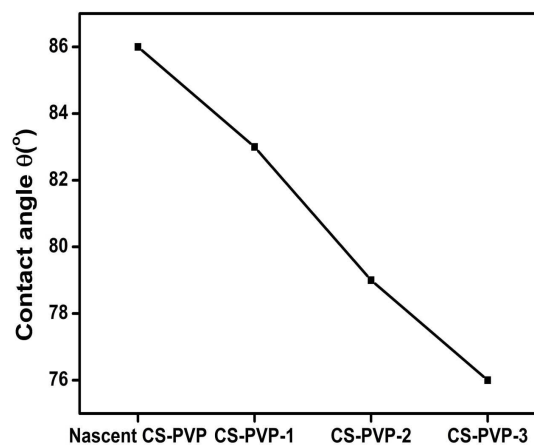


**Fig. 6** Change in water contact angle ( $\theta^\circ$ ) of nanocomposite membranes vs wt.% of GO loading, showing an increase in hydrophilicity with increasing GO loading.

### Equilibrium swelling

Figure 7 presents % equilibrium swelling (ES) results of nascent CS-PVP as well as other nanocomposite membranes at 30°C for 10 wt.% water containing ethanol feed mixtures. These studies are helpful to analyze free volume (tortuous pathways) of the matrix to solvent diffusion or permeation<sup>46</sup>. It is observed that with an increase in filler loading, there is a parallel increase in membrane swelling, which is due to enhanced membrane hydrophilicity. Compared to CS-PVP-2.5 (U), the CS-PVP-2.5 membrane showed higher swelling. This may be due to the fact that H<sub>2</sub>O<sub>2</sub> treatment increases number of oxygen functionality on graphene surface, thereby enhancing the number of active sites to facilitate water sorption, but uncontrolled membrane swelling can be avoided or reduced considerably by *glutaraldehyde* cross-linking.

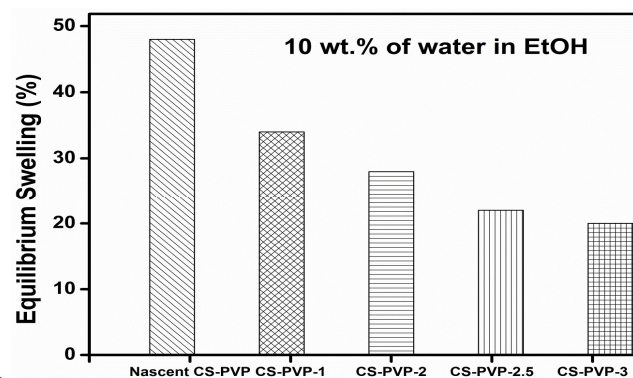


**Fig. 7** Equilibrium swelling (%) of membranes at 10 wt.% of water-EtOH mixture at 30°C, showing a decrease in swelling with increasing GO loading.

Table 1: Pervaporation data on membrane performance.							
Membrane type	Feed temp. (°C)	Equilibrium swelling (%)	Permeability (Barrer)	Selectivity ( $\alpha_{ij}$ )	$D_w \times 10^{-13}$ ( $m^2 s^{-1}$ )	$D_e \times 10^{-15}$ ( $m^2 s^{-1}$ )	
Nascent CS-PVP	30		85	152	2.9	22	
	40	48	87	135	2.8	24	
	50		93	123	3.2	30	
CS-PVP-1	30		93	294	3.1	12	
	40	34	97	236	3.5	17	
	50		103	212	3.7	20	
CS-PVP-2	30		99	624	3.2	6	
	40	28	102	472	3.7	9	
	50		114	405	4.0	11	
CS-PVP-2.5	30		105	955	3.4	4	
	40	22	108	749	3.8	6	
	50		118	499	4.3	10	
CS-PVP-3	30		117	584	3.8	7	
	40	20	122	439	4.6	12	
	50		128	366	5.2	16	
CS-PVP-2.5(U)	30		101	671	3.3	5	
	40	21	104	472	3.6	9	
	50		122	407	4.2	12	

### Membrane Performance

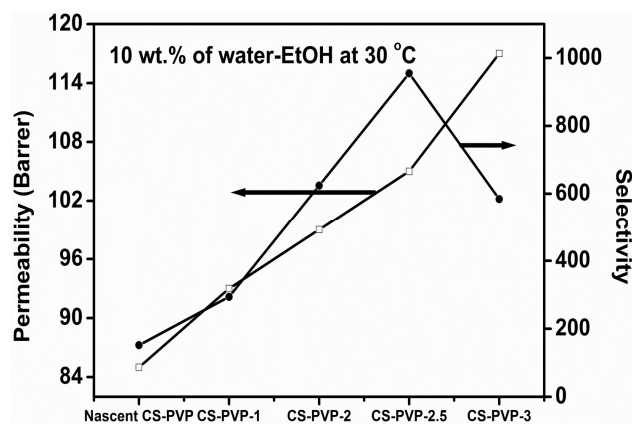
#### Effect of GO Loading

Figure 8 and Table 1 shows the effect of GO loading on PV performance of nanocomposite membranes at 30°C tested for 10 wt.% of water in ethanol feed mixture. As the GO loading increased from 1 to 2.5 wt.%, both permeability and selectivity increased. This could be attributed to favourable compatibility between GO and CS-PVP, due to uniform dispersion of GO

nanosheets into blend membrane matrix (as was also shown before by FE-SEM studies). Contact angle measurements also support that presence of GO particles in membrane interface surface increases the hydrophilic nature, leading to enhanced sorption selectivity. The GO helps as a reinforcing bridge in the blend matrix, resulting in tortuous pathways, thus enabling high water selective diffusivity. At a maximum loading of 2.5 wt.% of GO, optimum separation performance is observed and above this

limit particle agglomeration resulted and at 2.5 wt.% GO loading, the maximum selectivity observed is 955.

As observed in **Figure 8**, as the GO loading increased to 3 wt.%, the membrane selectivity value decreased sharply from 955 to 584. This is mainly attributed to increased defects induced by excess GO loading, which would strongly destroy interfacial adhesion between GO and polymer blend matrix. Even EtOH molecules may also permeate preferentially through such defects and loose interface spaces between GO and polymer blend matrix, which eventually might have led to increase in permeability at the cost of selectivity. Moreover, there might be two possible reasons contributed to the decline in selectivity: shortened transport route of penetrating components and more undetected defects in the membranes. The undetected effects (even by SEM) would occur since GO nanosheets cannot be neglected compared to the bulk of the membrane. These factors might also be responsible for observed decline in selectivity at high loading of GO.



**Fig. 8** Effect of filler loading on permeability (Barrer) and selectivity of nascent chitosan and GO loaded chitosan nanocomposite membranes at 10 wt.% of water-EtOH feed mixture.

#### Effect of $H_2O_2$ treatment

In order to further increase compatibility between graphene and the CS-PVP chains, GO nanosheets were treated with  $H_2O_2$ , which was found to enhance oxygen content of GO from  $C_{10}O_{0.78}H_{0.38}$  to  $C_{10}O_{0.99}H_{0.73}$  (as per elemental analysis). As depicted in **Figure 9**, the presence of additional oxygen functionalities seems to be instrumental in obtaining 40 % higher membrane selectivity along with a slight improvement in total permeability of the membranes. One of the main reasons for increased membrane performance after incorporation of GO is the presence of 'enhanced oxygen functionality' on graphene surface,

which would enhance both sorption and diffusion selectivity of the membrane.

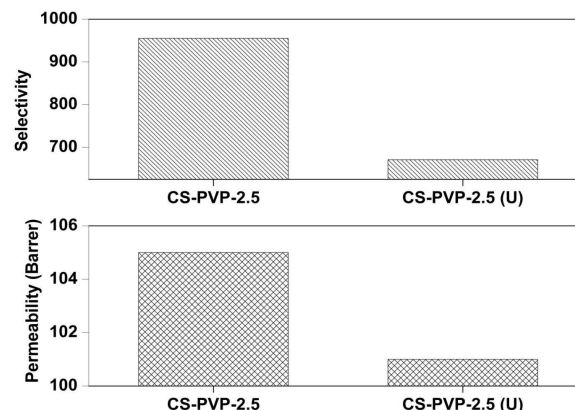


**Fig. 9** Comparison of membrane performance (selectivity and permeability) of CS-PVP-2.5 and CS-PVP-2.5 (U) for water-EtOH mixture.

Upon increasing the number of oxygen functionalities, interaction of graphene with water molecules will also increase along with an improvement in interface interaction with the polymer chains as per the interaction model proposed in **Figure 10**. Therefore, oxygen functionality of GO is responsible to improve the interface interaction with polymer chains; this can be evidenced by the improved values of sorption and diffusion selectivity of water.

#### Effect of operating temperature

**Figure 11a** displays the effect of operating temperature on PV performance typically in the case of CS-PVP-2 membrane for 10 wt.% water containing feed mixture. The operating temperature ranges of this study correspond to reasonable operating conditions of the PV process for ethanol dehydration. The permeability values increased from 99 to 114 Barrer, but the selectivity declined from 624 to 405. The increase in permeability at the loss of selectivity with temperature could be attributed to three reasons: One is that increased mobility of penetrating molecules in the bulk feed solution might have resulted in higher partial vapour pressure to provide higher driving force for permeating molecules, and this would facilitate transport of both liquid components in the membrane. The second is that flexibility of blend polymer segments get enhanced at rising temperature thus accelerating non selective diffusion of the components. In the case of GO-loaded membranes, variation of interface between polymer blend and GO induced by rising of the temperature would also play a major role as well.

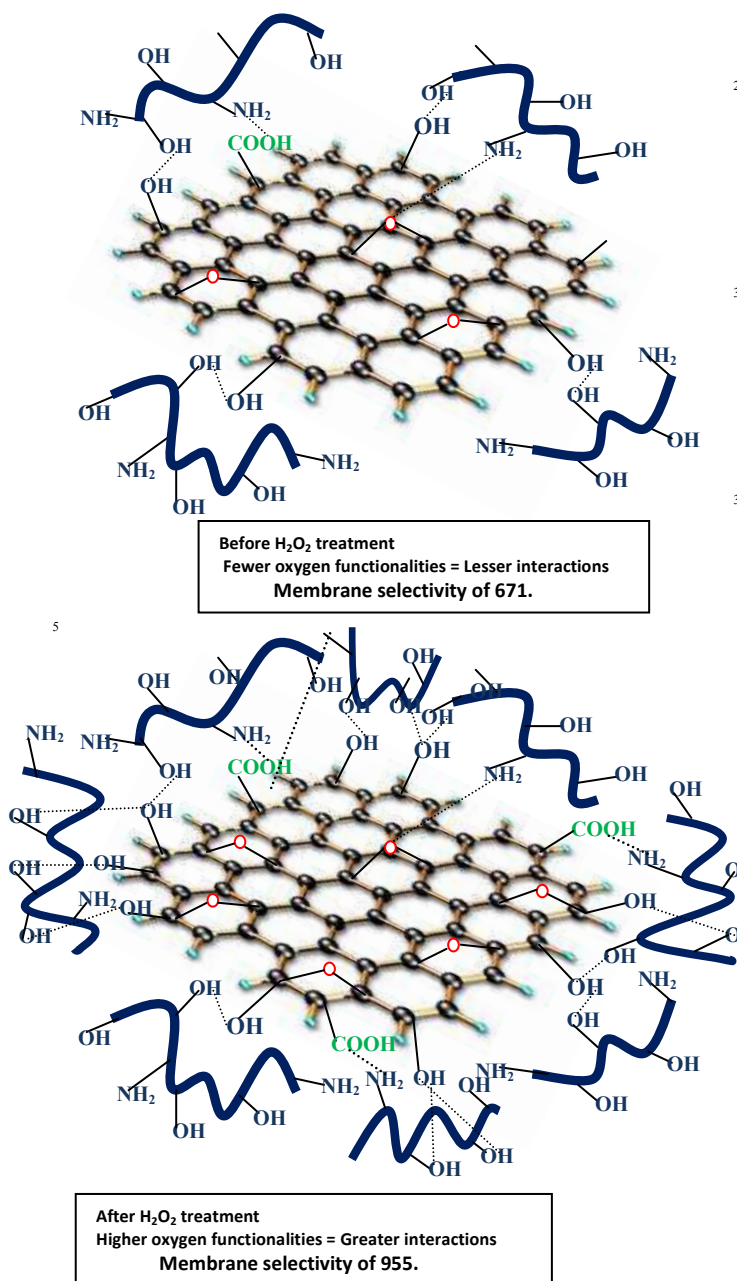


Fig. 10 The interaction models showing the effect of H<sub>2</sub>O<sub>2</sub> treatment.

In other words, enhanced thermal mobility of polymer segments at higher temperature would eventually create larger free volume in the matrix. As the free volume increases, permeation of water molecules as along with EtOH also increases, thus exhibiting non-selective mass transport. The temperature dependent permeation and diffusion values exhibit the Arrhenius trends that are quantified through the calculations of activation energy parameters for the temperature-dependent values of diffusion and permeability.

#### Effect of feed concentration:

Figure 11 b demonstrates the effect of feed concentration on PV dehydration performance of CS-PVP-2 membranes, wherein it is observed that increase in feed water composition increased the permeability at the cost of selectivity. This could be mainly attributed to enhancement in driving force followed by increase in membrane swelling. Increase in feed water composition would result in increase of water molecules on the feed side, while on permeate side it is being constantly removed, leading to increase of chemical potential gradient (driving force). The increase in equilibrium swelling with increasing feed water composition is responsible for increased membrane swelling, allowing the easier permeation of both water and EtOH molecules.

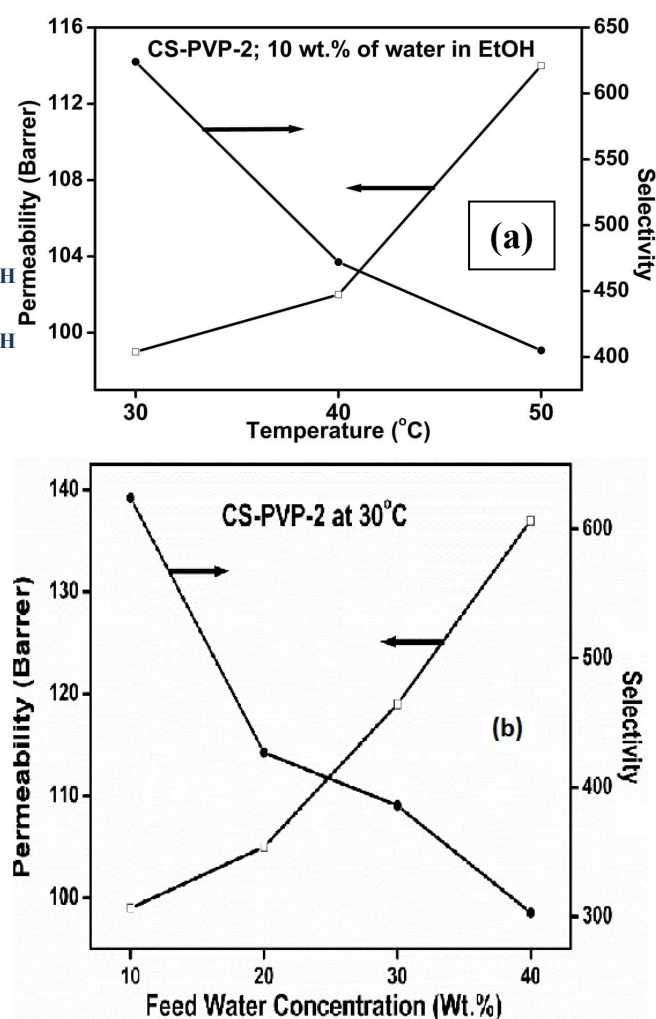


Fig. 11 Variation of permeability and selectivity of CS-PVP-2 membranes with (a) temperature at 10 wt.% of water in EtOH and (b) feed composition at 30°C.

### Arrhenius activation energy calculations

Arrhenius activation energy for permeability and diffusion processes of the feed mixture components have been calculated

$$X = X_o \exp\left(\frac{-E_x}{RT}\right) \text{----- (7)}$$

where  $X$  represents permeability ( $P$ ) or diffusion coefficient ( $D$ ),  $X_o$  is a constant representing pre-exponential factor,  $P_o$  or  $D_o$ ;  $E_x$  is activation energy for permeation or diffusion process,  $R$  is the universal gas constant and  $T$  is temperature in Kelvin. From the Arrhenius plots of  $\ln P_w / I$ , and  $\ln D_w$  vs  $1/T$  (not displayed to avoid overcrowding of figures) and from the least-squares fitting of the linear plots, activation energy values ( $kJ/mol$ ) for permeability of water ( $E_{pw}$ ) and EtOH ( $E_{pEtOH}$ ) were calculated. Similarly, activation energy for diffusion of water ( $E_{Dw}$ ) and EtOH ( $E_{DEtOH}$ ) were calculated. These data compiled in **Table 2** show lower diffusion energy barrier values for water compared to EtOH. After incorporating GO into the CS-PVP matrix, energy barrier for water declined, while that of EtOH increased, suggesting the water selective nature of the membranes. The decrease in water diffusion energy barrier can be observed up to 2.5 wt.% GO loading, and above this limit, trend is reversed, due to the possible particle agglomeration. On the other hand, H<sub>2</sub>O<sub>2</sub> treated GO loaded membranes showed much lower energy barrier values for water permeation than untreated graphene loaded membranes.

Heat of sorption values were calculated from the difference values of energy of activation for permeability and diffusion using:

$$\Delta H_s = E_{pi} - E_{Di} \text{----- (8)}$$

The calculated  $\Delta H_s$  values presented in **Table 2** suggest the nature of transport phenomenon, which involves the combined effect of Henry's and Langmuir's type of sorption phenomenon<sup>47</sup>. Henry's law implies that heat of sorption follows endothermic process for liquid transport, leading to dissolution of chemical species into that site within the membrane matrix. On the other hand, Langmuir's sorption requires pre-existence of a site into which sorption occurs by hole-filling mechanism to offer exothermic contribution. The  $\Delta H_s$  values obtained are negative (exothermic contribution) for all membranes, indicating that Langmuir's type of sorption is predominant in the present systems.

**Table 2** Arrhenius activation parameters ( $kJ\ mol^{-1}$ ).

Membranes	$E_{pw}$	$E_{Dw}$	$\Delta H_s$	$E_{pEtOH}$	$E_{DEtOH}$	$\Delta H_s$
Nascent CS-PVP	14.6	24.5	-9.9	35.2	47.0	-11.8
CS-PVP-1	11.8	23.2	-11.4	39.3	51.4	-12.1
CS-PVP-2	10.2	22.0	-11.8	40.8	54.3	-13.5
CS-PVP-2.5	8.1	19.8	-11.7	44.6	57.9	-13.3
CS-PVP-3	9.4	21.4	-12.0	42.0	55.2	-13.2
CS-PVP-2.5(U)	8.8	20.6	-11.8	43.2	56.4	-13.2

### Membrane-solvent interactions

The selective mass transport through dense polymeric membrane occurs through the combined effect of differential diffusion as well as physico-chemical interactions between liquid permeate molecules and polymer matrix due to sorption. Sorption phenomenon is a thermodynamic process, which determines how much of liquid get accommodated per unit volume into a polymer matrix. Equilibrium swelling data are used to calculate the Flory-Huggins interaction parameter ( $\chi_{ip}$ ) between the polymer and the liquid molecules using the following equation<sup>48</sup>:

$$\ln \alpha_i = \ln \phi_i + (1 - \phi_i) + \chi_{ip}(1 - \phi_i)^2 \text{----- (9)}$$

Here,  $\alpha_i$  is activity of solvent and subscript  $i$  refers to water or EtOH. The volume fraction,  $\phi_i$  was calculated from the equilibrium swelling data obtained in pure liquid media using:

$$\phi_i = \frac{W_i / \rho_i}{W_i / \rho_i + 1 / \rho_m} \text{----- (10)}$$

where  $\rho_i$  and  $\rho_m$  are densities of liquid and membrane, respectively;  $W_i$  is liquid uptake (g/g of dry membrane) of component  $i$  at equilibrium.

The membrane density ( $\rho_m$ ) was calculated by benzene-displacement method<sup>18</sup> as:

$$\rho_m = \frac{W_m}{V_b} \text{----- (11)}$$

where  $W_m$  is weight of the membrane and  $V_b$  is volume of benzene displaced. By using the  $\phi_i$  values,  $\chi_{ip}$  was calculated as<sup>49</sup>:

$$\chi_{ip} = -\left(\frac{\ln \phi_i + (1 - \phi_i)}{(1 - \phi_i)^2}\right) \text{----- (12)}$$

40

The parameter  $\chi_{ip}$  represents the chemical compatibility between liquid molecules,  $i$  (water or EtOH) and the membrane polymer,  $p$ .

By incorporating the  $\chi_{ip}$  values, membrane solubility parameter ( $\delta$ ) was calculated as:

$$\chi_{ip} = 0.35 + \frac{V_i}{RT} (\delta_i - \delta_p)^2 \quad \text{----- (13)}$$

where  $T$  is absolute temperature in Kelvin,  $R$  is universal gas constant ( $8.314 \text{ JK}^{-1}\text{mol}^{-1}$ ) and  $V_i$  is molar volume of the solvent;  $\delta_i$  and  $\delta_p$  are solubility parameters of liquid and polymer respectively. Taking the values of  $\delta$  for EtOH and water, respectively as  $23.6 \text{ J}^{1/2} \text{ cm}^{-3/2}$  and  $47.8 \text{ J}^{1/2} \text{ cm}^{-3/2}$ ,  $\delta_p$  of the polymer was calculated using Eq. (14), which was derived from

$$\text{Eq. (13)} \quad \delta_p = \delta_i \pm \left[ \frac{(\chi_{ip} - 0.35) RT}{V_i} \right]^{1/2} \quad \text{----- (14)}$$

Since sorption of membrane was measured in EtOH and water separately, we have chosen the one that matched better for the determination (here,  $i$  refers to water). Equation (14) has two roots and hence,  $\delta_p$  theoretically takes either of the two values while determining membrane-solvent solubility.

The lower  $\chi_{ip}$  values represent a stronger interaction between liquid media and the polymer. The results of **Table 3** show almost ten-times lower  $\chi_{1p}$  (water-polymer interaction) values than  $\chi_{2p}$  (EtOH-polymer interaction), confirming the water-selective nature of the membranes. Notice that by incorporating GO nanoparticles, the  $\chi_{1p}$  values have decreased dramatically, while those of  $\chi_{2p}$  values increased slightly. Such an effect is attributed to the added water-selective nature of GO nanosheets, which was also confirmed by water contact angle and equilibrium swelling data. By increasing the GO loading, the  $\chi_{1p}$  values decrease up to 2.5 wt.% of loading, above which the trend is reverted, due to attainment of saturation limit of GO in the membrane matrix. Comparatively,  $\text{H}_2\text{O}_2$  treated GO loaded membranes have shown the lower  $\chi_{1p}$  values than the corresponding untreated GO loaded membranes, due to increase in hydrophilicity of GO after its  $\text{H}_2\text{O}_2$  treatment. Similarly, the

$\delta_p$  values show increase with increased loading of GO nanosheets, indicating increased hydrophilicity of the membrane. The  $\delta_p$  values of  $\text{H}_2\text{O}_2$  treated GO loaded membranes showed higher values of  $\delta_p$  than those of the unmodified GO-loaded membranes, which is due to the overall enhancement of polar nature (hydrophilicity) of the membranes.

#### Molar mass between cross-links and cross-link density

The molar mass between cross-links ( $M_c$ ) and crosslink density ( $v_e$ ) of the polymers were calculated as<sup>50</sup>:

$$\frac{1}{M_c} = - \frac{(1/\rho_p V_i) [\ln(1-\phi_i) + \phi_i + \chi_{ip} \phi_i^2]}{\phi_i^{1/3} - (1/2)\phi_i} \quad \text{----- (15)}$$

$$v_e = \frac{\rho_m}{M_c} \quad \text{----- (16)}$$

Usually, cross-linked polymers show higher  $v_e$  and lower  $M_c$  values. As per the data given in **Table 3**, the decreasing  $M_c$  values with increasing  $v_e$  with increased GO loading, indicating enhanced membrane packing density, which could be due to the presence of polar groups on both CS/PVP blend and GO, leading to multiple H-bonded sites (interaction model). The increase in packing density was observed up to 2.5 wt.% of GO loading and above this limit the trend reverted, since membranes attained saturation limit at 2.5 wt.% loading. On the other hand,  $\text{H}_2\text{O}_2$  treated GO loaded CS/PVP blend nanocomposite membranes show higher cross-link densities than the unmodified GO loaded membranes as a result of improved interfacial compatibility between the GO nanosheets and the CS/PVP blend polymer after  $\text{H}_2\text{O}_2$  treatment of GO.

**Table 3** Thermodynamic data on membrane mixed media interaction.

Membranes	F-H parameters		$\delta_p$ (J <sup>1/2</sup> cm <sup>-3/2</sup> )	$M_c$ (g/mol)	$V_c \times 10^3$ (mol/cm <sup>3</sup> )
	$\chi_{1p}$	$\chi_{2p}$			
Nascent CS-PVP	-19	-3.7	100	474	3.2
CS-PVP-1	-29	-3.4	112	262	6.2
CS-PVP-2	-34	-3.2	117	222	7.6
CS-PVP-2.5	-37	-2.9	121	199	8.6
CS-PVP-3	-35	-3.2	119	227	7.8
CS-PVP-2.5(U)	-34	-3.0	118	221	7.5

### 5 Diffusion coefficient

Diffusion is a kinetic parameter, which determines the rate at which liquid molecules diffuse through the membrane. Diffusion coefficient (concentration independent) can be calculated as:

$$D_i = \frac{P_i}{K_i} \quad \text{----- (17)}$$

10 where  $K_i$  is sorption coefficient and  $P_i$  is permeation flux/unit area (kg/m<sup>2</sup>s) of the  $i^{\text{th}}$  component (water or EtOH) inside the membrane matrix (m<sup>3</sup> (STP) m<sup>-3</sup> mmHg<sup>-1</sup>). The values of  $K_i$  are calculated using:

$$K_i = \frac{C_i}{p_i} \quad \text{----- (18)}$$

15 Here,  $C_i$  stands for liquid concentration inside the membrane and  $p_i$  is partial pressure of the  $i^{\text{th}}$  component.

All the membranes show (see **Table 1**) two orders of magnitude higher diffusion selectivity towards water molecules than EtOH molecules. With an increase in GO loading, diffusion of water molecules increased, giving decrease in permeation of EtOH molecules. The tortuous diffusion pathways created in the matrix could facilitate permeation of smaller water molecules than EtOH. The increasing trend of water diffusion is below 2.5 wt.% GO loading and after this limit, the trend was reverted. 20 Comparatively, nanocomposite membranes containing H<sub>2</sub>O<sub>2</sub> treated GO shows better diffusion selectivity than untreated graphene sheets containing membranes. The feed parameters such as increase of water composition and temperature have affected adversely on the diffusion selectivity, of membranes.

### Conclusions

One of the main concerns of graphene composite membranes in PV application is its low compatibility with a polymer matrix.

In this work, we have attempted to address this issue by using 35 H<sub>2</sub>O<sub>2</sub> treated graphene by incorporating into a CS/PVP blend matrix and these membranes when tested for PV dehydration of ethanol as a function of GO loading, feed composition and feed temperature, showed improved results. The H<sub>2</sub>O<sub>2</sub> treatment of GO enhanced the number of oxygen functionalized polar sites 40 onto graphene surface, which has enhanced sorption and diffusion selectivity. The FE-SEM micrographs combined with XRD confirmed for good interface compatibility between GO nanosheets and CS/PVP blend polymer. FTIR spectra proved enhanced H-bonding interactions, while contact angle studies 45 proved increase in hydrophilicity of membranes with increased GO loading. TGA and DSC studies proved enhancement of membrane thermal stability with increasing GO loading. The interaction parameter ( $\chi$ ) and diffusion coefficient values supported the progressive improvement of selectivity and 50 permeability data with GO loading. Membranes attained optimum concentration at 2.5 wt.% loading, but any further increase of GO loading resulted in a decrease of membrane performance. Overall, the H<sub>2</sub>O<sub>2</sub> treatment proved to be effective to enhance PV performance of the nanocomposite membranes.

### Acknowledgements

Financial assistance from Department of Atomic Energy (DAE), Board of Research in Nuclear Sciences (BRNS) (Grant 2013/34/BRNS), Admar Mutt Education Foundation (AMEF), 60 Bangalore, Dr. K. Venkatesh, Director, CET, Jain University are gratefully acknowledged. Dr. Suhas D. P. is thankful to Council for Scientific and Industrial Research for awarding Senior Research Fellowship (F.N09/1052(0004)2K14-EMR-I).

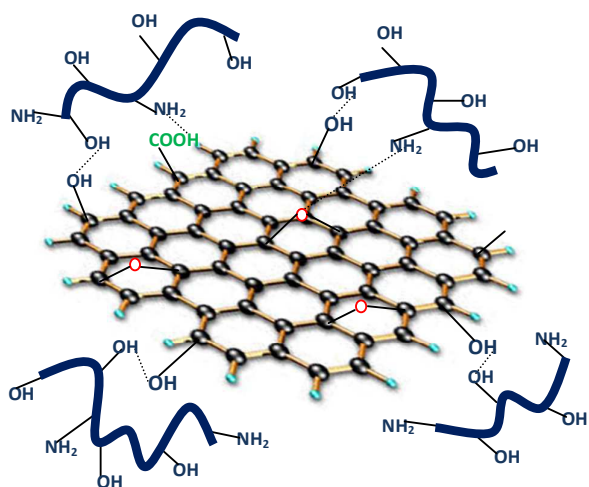
### References

1. D. Tilman, J. Fargione, B. Wolff, C. D'Antonio, A. Dobson, R. Howarth, D. Schindler, W.H. Schlesinger, D. Simberloff, *Science*, 2001, **292**, 281-284.
2. D. Tilman, K.G. Cassman, P.A. Matson, R. Naylor, S. Polasky, *Nature*, 2002, **418**, 671-677.
3. REN21. Renewables 2012 Global Status Report; *REN21 Secretariat*, 2012.
4. C.N. Hamelinck, G. Van Hooijdonk, A.P.C. Faaij, *Biomass Bioenergy*, 2005, **28**, 84-410.
5. L.R. Lynd, *Rev. Energy Environ.*, 1996, **21**, 403-465.

6. S.D. Bhat, T.M. Aminabhavi, *Microporous Mesoporous Mater.*, 2006, **91**, 206-214.
7. S.D. Bhat, B.V.K. Naidu, G.V. Shanbag, S.B. Halligudi, T.M. Aminabhavi, *Sep. Purif. Technol.* 2006, **49**, 56-63.
8. B. Bolto, M. Hoang, Z. Xie, *Chem. Eng. Process.* 2011, **50**, 227-235.
9. D. Anjali Devi, B. Smitha, S. Sridhar, T.M. Aminabhavi, *J. Memb. Sci.* 2006, **280**, 45-53.
10. M. Rinaudo, *Prog. Poly. Sci.*, 2006, **31**, 603-632.
11. S.S. Jawalkar, S.G. Adoor, M. Sairam, N.N. Mallikarjuna, T.M. Aminabhavi, *J. Physical Chem. B* 2005, **109**, 15611-15620.
12. T. Uragami, K. Okazaki, H. Matsugi, T. Miyata, *Macromolecules*, 2002, **35**, 9156-9163.
13. V.T. Magalad, G.S. Gokavi, C. Ranganathaiah, M.H. Burshe, C. Han, D.D. Dionysiou, M.N. Nadagouda, T.M. Aminabhavi, *J. Memb. Sci.* 2013, **430**, 321-329.
14. S.D. Bhat, T.M. Aminabhavi, *Sep. Purif. Technol.* 2006, **51**, 85-94.
15. S.G. Adoor, B. Prathab, L.S. Manjeshwar, T.M. Aminabhavi, *Polymer*, 2007, **48**, 5417-5430.
16. S.G. Adoor, M. Sairam, L.S. Manjeshwar, K.V.S.N. Raju, T.M. Aminabhavi, *J. Membr. Sci.* 2006, **285**, 182-195.
17. D.P. Suhas, T.M. Aminabhavi, A.V. Raghu, *Appl. Clay Sci.* 2014, **101**, 419-429.
18. V.T. Magalad, G.S. Gokavi, K.V.S.N. Raju, T.M. Aminabhavi, *J. Membr. Sci.* 2010, **354**, 150-161.
19. D.P. Suhas, T.M. Aminabhavi, A.V. Raghu, *Polym. Eng. Sci.* 2014, **54**, 1774-1782.
20. D.Y. Kang, H.M. Tong, J. Zang, R.P. Choudhury, D.S. Sholl, H.W. Beckham, C.W. Jones, S. Nair, *ACS Appl. Mater. Interfaces*, 2012, **4**, 965-976.
21. C.H. Kang, Y.F. Lin, Y.S. Huang, K.L. Tung, K.S. Chung, J.T. Chen, W.S. Huang, K.R. Lee, J.Y. Lai, *J. Membr. Sci.* 2013, **438**, 105-111.
22. G. Liu, D. Yang, Y. Zhu, J. Ma, M. Nie, Z. Jiang, *Chem. Eng. Sci.* 2011, **66**, 4221-4228.
23. Y. Shirazi, T. Mohammadi, *Sep. Sci. Technol.* 2013, **48**, 716-727.
24. D.P. Suhas, A.V. Raghu, H.M. Jeong, T.M. Aminabhavi, *RSC Adv.* 2013, **3**, 17120-17130.
25. C.N.R. Rao, A.K. Sood, K.S. Subrahmanyam, A. Govindaraj, *Angew. Chem.* 2009, **48**, 7752-7777.
26. T. Kuilla, S. Bhadra, D. Yao, N.H. Kim, S. Bose, J.H. Lee, *Prog. Poly. Sci.* 2010, **35**, 1350-1375.
27. Z. Jia, Y. Wang, *J. Mater. Chem. A* 2015, **3**, 4405-4412.
28. X. Chang, Z. Wang, S. Quan, Y. Xu, Z. Jiang, L. Shao, *Appl. Sur. Sci.* 2014, **316**, 547-548.
29. L. Shao, X. Cheng, Z. Wang, J. Ma, Z. Guo, *J. Memb. Sci.* 2014, **452**, 82-89.
30. H.M. Hegab, L. Zou, *J. Memb. Sci.* 2015, **484**, 95-106.
31. L. Shao, X. Chang, Y. Zhang, Y. Huang, Y. Yao, Z. Guo, *Appl. Sur. Sci.* 2013, **280**, 989-992.
32. C-H. Tsou, Q-F. An, S-C. Lo, M. D. Guzman, W-S. Hung, C-C. Hu, K-R Lee, J-Y. Lai, *J. Memb. Sci.* 2015, **477**, 93-100.
33. R.R. Nair, H.A. Wu, P.N. Jayaram, I.V. Grigorieva, A.K. Geim, *Science*, 2012, **335**, 442-444.
34. K. Huang, G. Liu, Y. Lou, Z. Dong, J. Shen, W. Jin, *Angew. Chem.* 2014, **53**, 6929-6932.
35. D.P. Suhas, A.V. Raghu, H.M. Jeong, T.M. Aminabhavi, *Ind. Eng. Chem. Res.* 2014, **53**, 14474-14484.
36. J.T. Choi, T.D. Dao, K.M. Oh, H-il. Lee, H.M. Jeong, B.K. Kim, *Smart Mater. Struct.* 2012, **21**, 75017.
37. T.M. Aminabhavi, R.S. Khinnavar, *Polymer* 1993, **34**, 1006-1018.
38. T.M. Aminabhavi, H.G. Naik, *J. Appl. Poly. Sci.* 2002, **83**, 244-258.
39. R.W. Baker, J.G. Wijmans, Y. Huang, *J. Membr. Sci.* 2010, **348**, 346-352.
40. V.T. Magalad, G.S. Gokavi, N.N. Mallikarjuna, B. Prathab, T.M. Aminabhavi, *J. Phys. Chem. C*, 2011, **115**, 14731-14744.
41. S.G. Adoor, S.D. Bhat, D.D. Dionysiou, M.N. Nadagouda, T.M. Aminabhavi, *RSC Adv.* 2014, **4**, 52571-52582.
42. J.G. Wijmans, *J. Membr. Sci.* 2003, **220**, 1-3.
43. Gmehling, Onken, Arlt, 1977. *Ind. Eng. Chem.* 1970, **62**, 21-31.
44. G. Wang, B. Wang, J. Park, J. Yang, X. Shen, J. Yao, *Carbon*, 2009, **47**, 68-72.
45. T.M. Aminabhavi, R.S. Khinnavar, S.B. Hargoppad, U.S. Aithal, Q.T. Nguyen, K.C. Hasan, *J. Macromol. Sci. C*, 1994, **34**, 139-204.
46. D.H. Weinkauf, D.R. Paul, *ACS Symp. Ser.* 1990, **423**, 61-91.

- 
47. T.M. Aminabhavi, P. Munk, *Macromolecules*, 1979, **12**, 607-613.
  48. B. Prathab, V. Subramanian, T.M. Aminabhavi, *Polymer*, 2007, **48**, 409-416.
  - 5 49. G.M. Bristow, W.F. Watson, *Trans. Faraday Soc.*, 1958, **54**, 1731-1741.
  50. N.L. Le, T-S. Chung, *J. Memb. Sci.*, 2014, **454**, 62-73.

## Graphical Abstract:

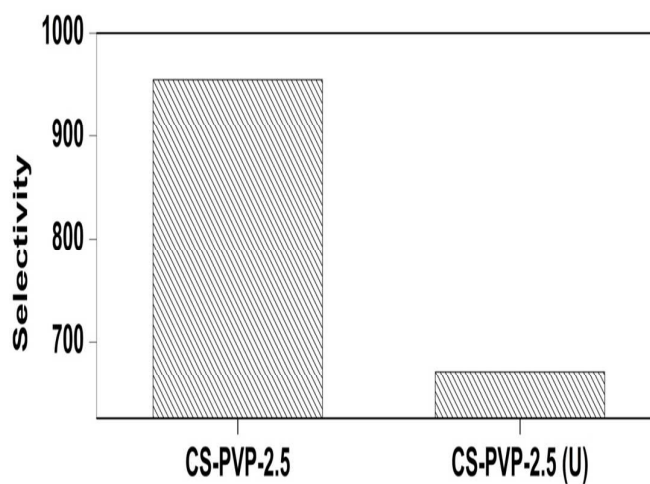
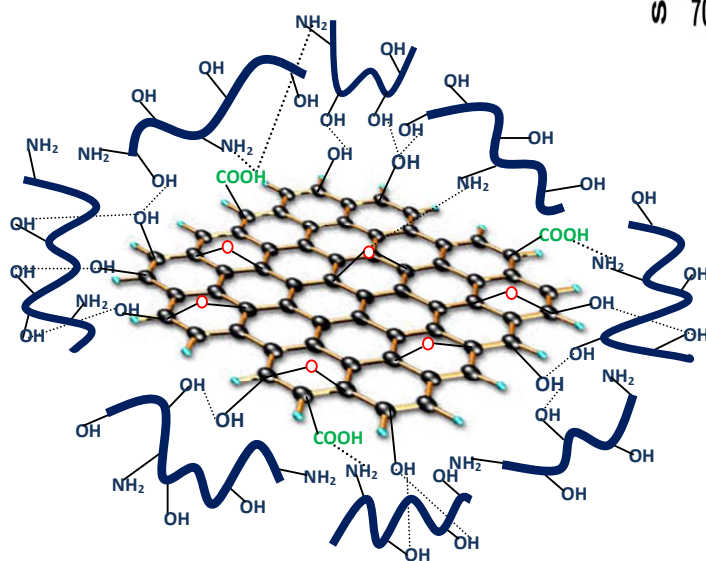


Fewer oxygen functionalities =  
Lesser interactions

Membrane selectivity of 671

(CS-PVP-2.5 (U))

After  $H_2O_2$  treatment



Higher oxygen functionalities =  
Greater interactions

Membrane selectivity of 955

(CS-PVP-2.5)